Earthquake detection through cross-correlation of the Stanford Fiber Seismic Observatory (SFSO) data

Siyuan Yuan, Biondo Biondi and Robert G. Clapp

ABSTRACT

Earthquakes occurring in similar locations can have repeatable waveforms. We show that with the Stanford Fiber Seismic Observatory (SFSO) earthquake recordings of Ladera and Felt Lake earthquakes as templates, we can detect other earthquakes occurred in similar locations through cross-correlation. As a benchmark, we applied cross-correlation to the recordings of the nearby seismometer stations. We found that the cross-correlation results of the SFSO recordings tend to have higher signal-to-noise ratios (SNR) and fewer false positives compared with the seismometer results. We also show that the SFSO is more sensitive to differences in earthquake mechanisms occurring in Ladera area compared to the two broadband stations. Through cross-correlation of the SFSO data, we identified two Felt Lake earthquakes that were not recorded in the United States Geological Survey (USGS) online catalog. With Felt Lake event recordings, we computed the amplitude ratios of the template to the four detected events. The ratios are similar to those computed with broadband stations for the two relatively large events, which shows the potential of magnitude estimation with SFSO data. For other two events, that are too weak to be included in the USGS catalog, SFSO tends to underestimate the ratios.

INTRODUCTION

Distributed Acoustic Sensing (DAS) holds great promise for application in cost-effective monitoring of microseismic signals and detecting earthquakes. Unlike the mainstream work previously done using DAS (e.g., using fibers in wells or burying the array in trenches), the Stanford Fiber Seismic Observatory (SFSO) uses a fiber-optic cable laying in an already existing polyvinyl chloride (PVC) conduit buried in the ground that makes the installation more convenient and economic (Martin et al., 2017a; Biondi et al., 2017). Understanding how well this type of cost-effective array records seismic events is one of our first-order objectives. With a repeatability analysis, we showed that our SFSO DAS array records coherent signals from earthquakes and quarry blasts occurred in the similar locations and with presumably similar mechanisms (Biondi et al., 2017; Yuan et al., 2017; Martin et al., 2017b). Yuan et al. (2017) showed that with cross-correlation we can find a time shift to cancel out

the waveforms of two Ladera earthquakes with coherent waveforms, which validates that the SFSO records coherent signals and demonstrates that cross-correlation can be potentially used as a template-matching approach to identify new earthquakes.

One major advantage of our DAS array is the cheap cost per sensor enabling a dense channel distribution. With hundreds of traces to average out the noise and enhance the signal, it has the potential, to some extent, to outperform 3C traditional seismometers with sparse channel distributions in detecting small and nearby earthquakes.

The cross-correlation amplitude between the events with similar epicenters and mechanisms can reflect the SNR level and sensitivity of our array to weak and nearby earthquakes. Li and Zhan (2018) demonstrate that with cross-correlation on SFSO data recorded in the Brady Hot Springs geothermal field, microseismicity below the noise level can be detected. Herein, we investigate if through cross-correlation of the SFSO recordings, we can detect events with similar epicenters and mechanisms. Then, to understand how well the detected events are correlated with the templates, we compare the cross-correlation results with those obtained from two nearby broadband stations - Jasper Ridge Seismic Station (JRSC) and Stanford Telescope Station (JSFB). The comparison of the correlated value can show the SNR level and the sensitivity of our array relative to the broadband stations. In the end, we compute the amplitude ratios of the Felt Lake template to each of the four detected Felt Lake events. We compare the ratios with the results obtained from the data of JRSC and JSFB to illustrate whether SFSO recordings can be effectively used to estimate the magnitude of the nearby weak events.

RECORDINGS OF THE LADERA AND FELT LAKE EARTHQUAKES

Martin et al. (2017a) provide most of the relevant information on the SFSO experiment. Figure 1 shows a simplified geometry of the SFSO array, namely six segments spreading out into two directions, colored in red and blue, respectively. The data displayed in the following sections have channels in same segments grouped together to see the move-out in each segment more conveniently. The channel spacing is 4 meters and the sampling rate is 50 samples per second. According to the USGS online catalog, two places close to the Stanford campus - Felt Lake and Ladera - have three and five small earthquakes, respectively since our SFSO array started recording. The following list provides the main information for the eight events - *Lad#1* through *Fl#3*. The event time (UTC), magnitude (M) and depth (z) of each event are based on the online USGS database. Distance (Δ) to our SFSO array of each event is calculated based on the 3D distance between the SFSO and the epicenter. *Fl#4* and *Fl#5* are two events detected by cross-correlation as described in the following sections. Both of them occurred in Felt Lake area. The event times for these two events are from the cross-correlation results. Since they are not included by the USGS online catalog, no metadata of the two events are available to us.

- *Lad#1*: 2017-08-10 03:19:47 – M1.79 – z=+3.25 km – Δ=4.62 km
- *Lad#2*: 2017-08-10 02:53:50 – M1.63 – z=+3.63 km – Δ=4.62 km
- *Lad#3*: 2017-11-27 15:30:45 – M1.94 – z=+3.64 km – Δ=5.37 km
- *Lad#4*: 2018-01-23 17:30:54 – M1.66 – z=+4.01 km – Δ=5.38 km
- *Lad#5*: 2017-01-11 23:04:40 – M2.03 – z=+4.15 km – Δ=5.75 km
- *Fl#1*: 2017-07-12 18:46:41 – M1.34 – z=+3.24 km – Δ=5.45 km
- *Fl#2*: 2017-07-12 18:47:50 – M0.95 – z=+3.05 km – Δ=5.34 km
- *Fl#3*: 2017-07-13 04:02:49 – M0.81 – z=+3.64 km – Δ=5.72 km
- *Fl#4*: 2017-05-10 06:35:38 – M???? – z=????? km – Δ=???? km
- *Fl#5*: 2017-07-13 05:56:06 – M???? – z=????? km – Δ=???? km

Figure 2 shows the locations of the eight epicenters and rough distances between the SFSO and Felt Lake and Ladera.

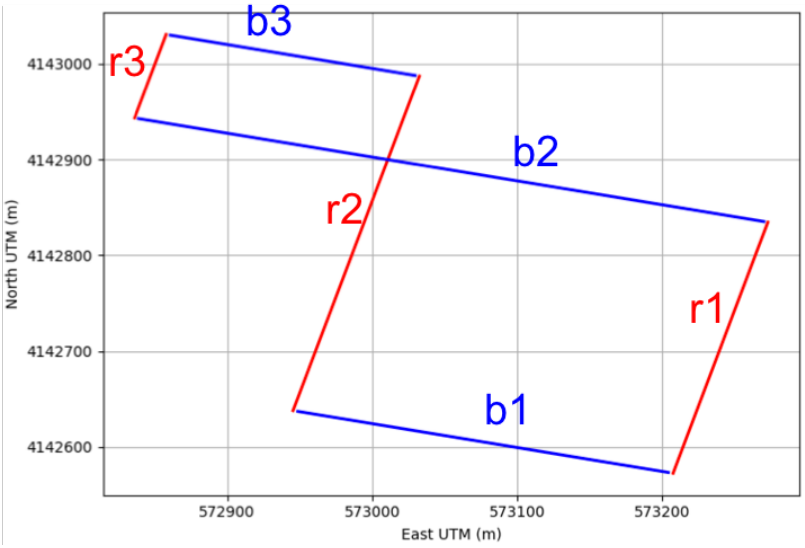

Figure 1: The layout of the simplified SFSO channel map. The fibers are extended into two directions colored in blue and red, respectively. 534 channels are distributed with a spacing of 4 meters along each line in the plot. The three vertical segments in the map are denoted by letters from r1 to r3. The three horizontal segments are denoted by letters from b1 to b3. [**ER**]

Figures 3 and 4 show the recordings of our SFSO array along with the vertical components of the two broadband stations, JRSC and JSFB, respectively. The SFSO recordings are shown in six segments separated by red and blue dash lines and a

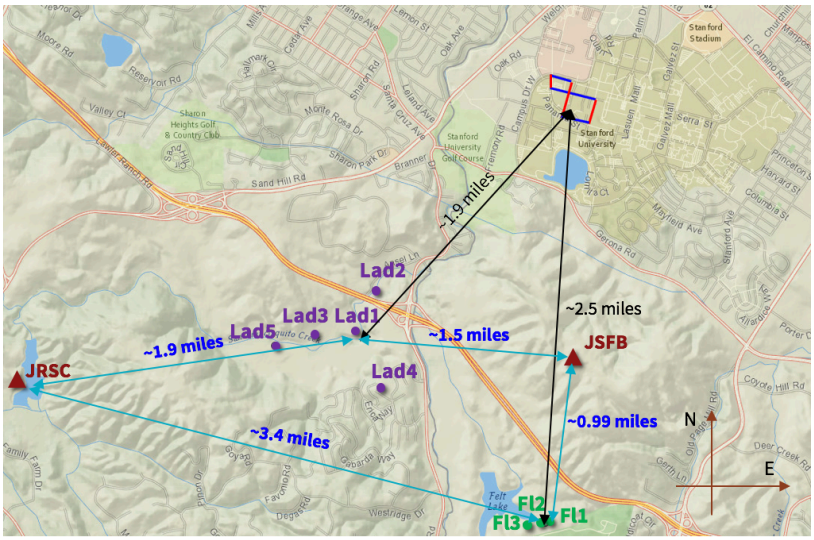

Figure 2: Epicenters of five Ladera earthquakes and three Felt Lake earthquakes are labeled on the map in purple and green, respectively. The distance from the SFSO array to the Ladera area is 1.9 miles, while the distance to the Felt Lake is 2.5 miles. The brown triangles show the locations of the two broadband stations, JRSC and JSFB. The distances from the broadband stations to the epicenters are indicated in the plot. [**NR**]

black line separating the two directions of fibers. The labels of the segments correspond to the labels shown in Figure 1. Zero time of the time axis corresponds to the event occurring time according to the USGS. Because the locations of the stations are different and the near-surface conditions and ray paths are different, the waveforms are not directly comparable. However, JRSC and JSFB data provide a rough indication of the arrival time and relative strength of the signal corresponding to different arrivals. Herein, we used *Lad#1* and *Fl#1* as templates to perform cross-correlation since they have the clearest waveforms among the other recordings cataloged by USGS. We chose 10-second time windows to include the waveforms and noise before and after the wave arrival to capture the characteristics of the waveforms and energy changes before and after the events arrive.

CROSS-CORRELATION

The first step is to develop an appropriate way to perform cross-correlation. We tried the events in the USGS catalog, which are listed in the previous section, to see if cross-correlation can detect them with enough confidence. SFSO data shown in Figure 3 and Figure 4 can be thought of as two-dimensional (2D) matrices, with a time axis and a channel number axis. We first performed 2D cross-correlation: looping a 10-second time window through the continuous data and computing the summation of the element-wise product of the 2D matrices of the time window and

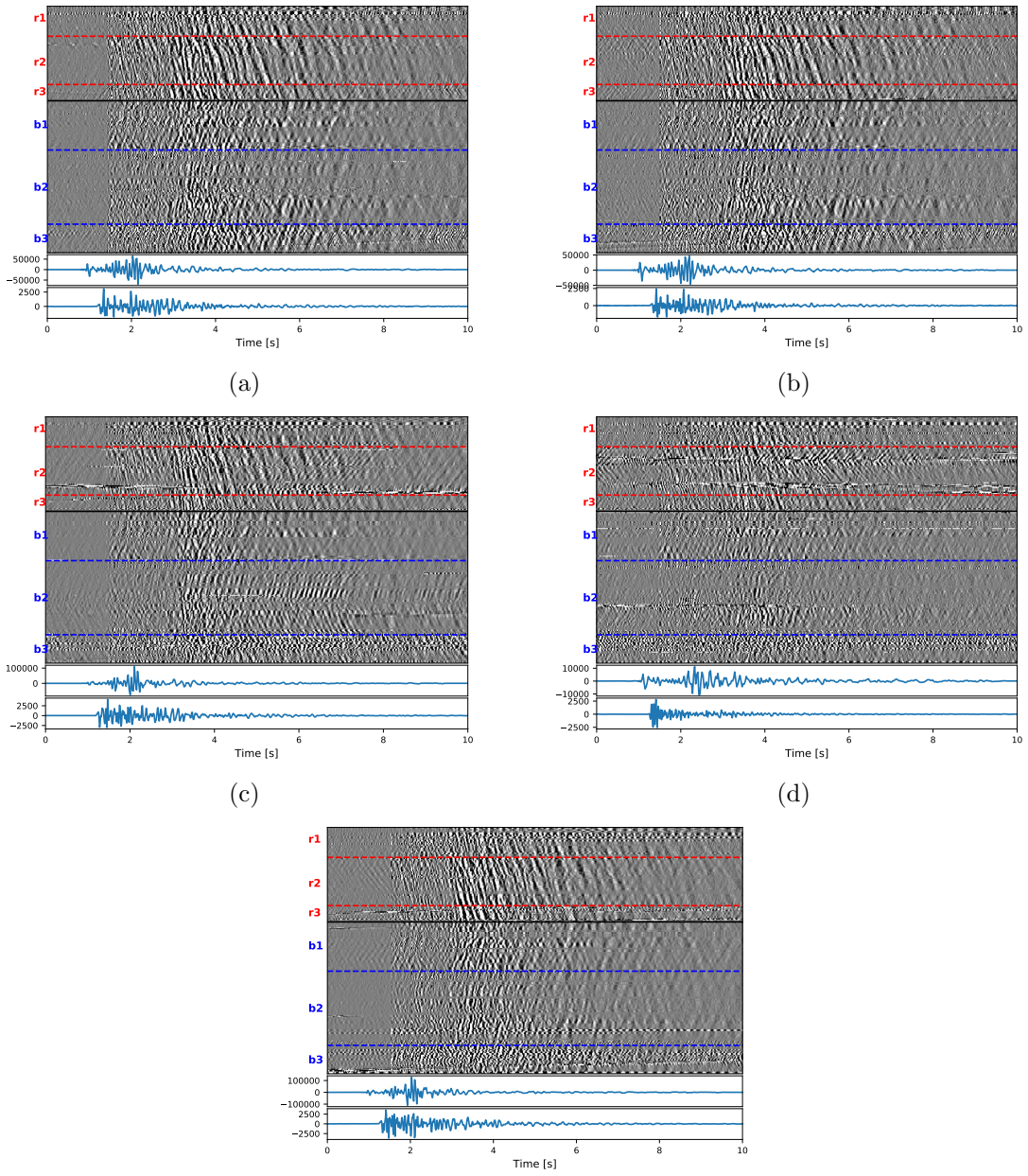

Figure 3: (a) to (e) show the data from *Lad#1* to *Lad#5* , respectively. The data shown in (a) is the template we use to perform cross-correlation. In each panel, a 2D plot shows our SFSO recording which is shown in six segments separated by red and blue dash lines and a black line separating the two directions of fibers. Each of the SFSO recordings has been clipped independently at 98 percentile. The vertical component of JRSC highpassed by 1.5 Hz is shown immediately following the SFSO data. The vertical component of the JSFB is shown in the bottom. Zero time on the time axis corresponds to the event occurring time according to the USGS. [**ER**]

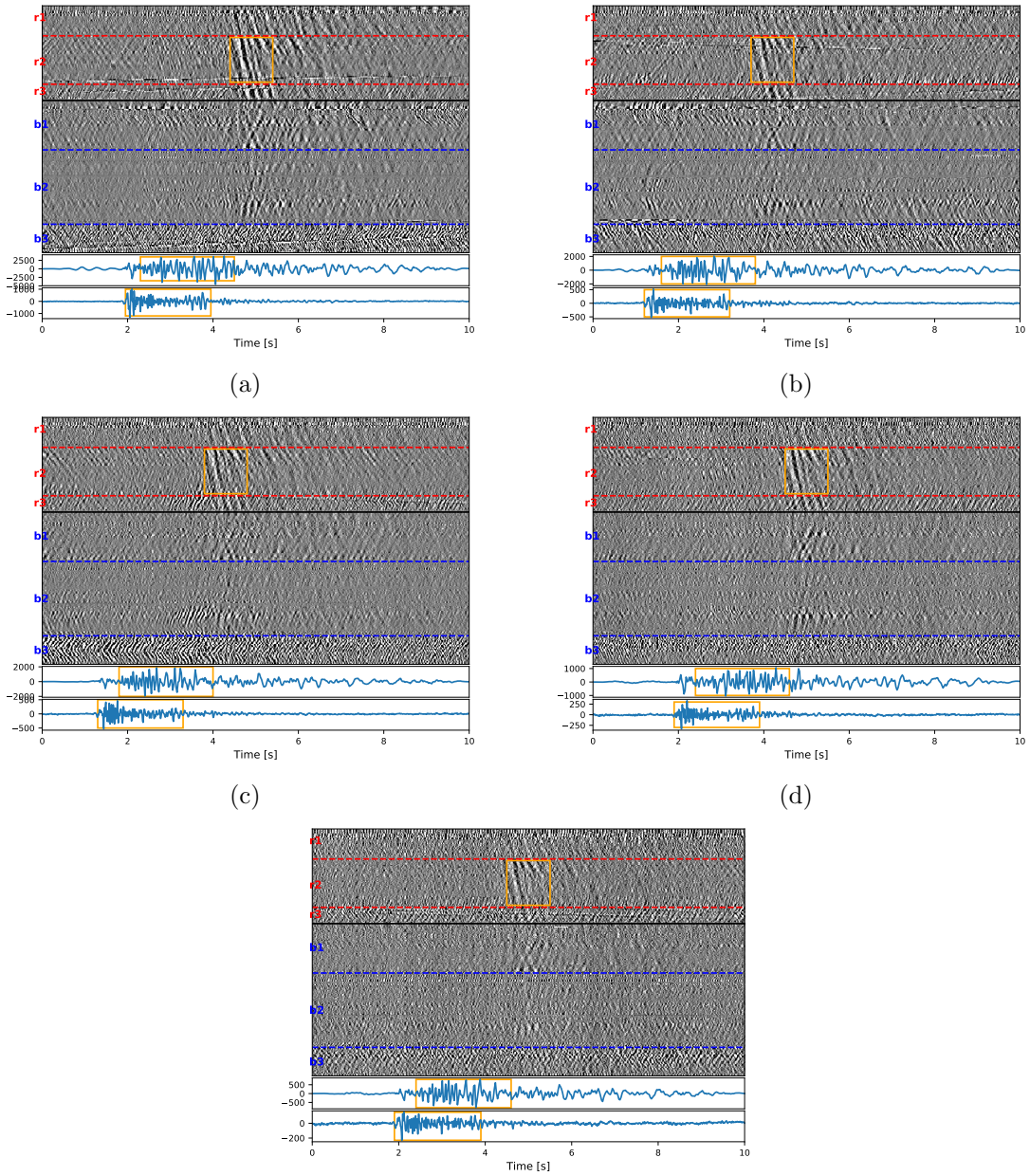

Figure 4: (a) to (e) show the data for *Fl#1*, *Fl#2*, *Fl#3*, *Fl#4* and *Fl#5*, respectively. The data shown in (a) is the template we use to perform cross-correlation. In each panel, a 2D plot shows our SFSO recording which is shown in six segments separated by red and dash lines and a black line separating the two directions of fibers. Each of the SFSO recordings has been clipped independently at 98 percentile. The vertical component of JRSC highpassed by 1.5 Hz is shown immediately following the SFSO data. The vertical component of the JSFB is shown in the bottom. Zero time on the time axis corresponds to the event occurring time according to USGS. The data surrounded by orange rectangles are used to compute the amplitude ratios as described in following sections. [**ER**]

the template. The operation is known as matrix Frobenius inner product. Then the product is normalized with respect to the Frobenius norm of the two matrices to only consider the patterns or the shape of the data instead of the absolute value. With the normalization, the cross-correlation value ends up being -1 to 1. For comparison, we performed one-dimensional (1D) cross-correlation on the vertical component of the broadband data because the vertical component has the highest SNR among all the other components. However, the 2D cross-correlation of the SFSO data produces great false positives. Figure 5a shows the cross-correlation of the Ladera event template on the continuous data recorded on August 10, 2017. From the previous section, we see that there is a weaker Ladera event with a magnitude of 1.6 (*Lad#2*), 26 minutes before the template event. The peak with an amplitude of 1 corresponds to the template. The other peak on the left with amplitude approximately 0.7 corresponds to the *Lad#2*. *Lad#2* stands out from the noise. But we also notice there are a few small spikes with amplitude approximately 0.1. It turns out that those spikes correspond to noise data instead of events. From Figure 6b and Figure 6c, which show the cross-correlation of broadband stations on the same time range, we do not see those small spikes at the corresponding time lags as we see in the SFSO results. The reason why these small spikes show up is because 2D correlation can be considered as the average of the trace-wise correlation which can be affected by the outliers of the trace-wise correlations. Those small spikes may correspond to the time window with high coherent noise in some traces, acting as outliers to pull up the 2D correlation results. Thus, instead of performing a 2D cross-correlation, we performed a trace-wise 1D cross-correlation; and then, we picked the median of those values to be more robust to outliers while at the same time taking advantage of the dense channel distribution of our SFSO array. The results of picking the median of trace-wise cross-correlation at each time lag are shown in Figure 5b. The evaluate the cross-correlation results here and in later discussions, we define the **average noise level** of cross-correlation results to be the 99.95 percentile of the absolute values of the cross-correlation of the template event with the whole 24-hour continuous recordings. And we define the **signal level** of cross-correlation to be the peak value of cross-correlation between template and another event occurring in similar location and with similar mechanisms (e.g. peak value of 0.8 of the spike corresponding to *Lad#2* in Figure 5b). The **SNR** is defined as the ratio between the signal level to the average noise level. As can be seen, the SNR is evidently higher compared with Figure 5a. Thus, in the later analysis, we adopted the median cross-correlation method.

CROSS-CORRELATION WITH THE LADERA TEMPLATE

Figure 6 shows the comparison between the cross-correlation of SFSO and the two broadband stations for the data recorded on August 10, 2017, when *Lad#1* and *Lad#2* occurred. All three instruments have *Lad#2* detected at the right timing. *Lad#2* corresponds to the second strongest spike in each panel. As can be seen, JRSC has a few spikes that are false positives and are not detectable in the other

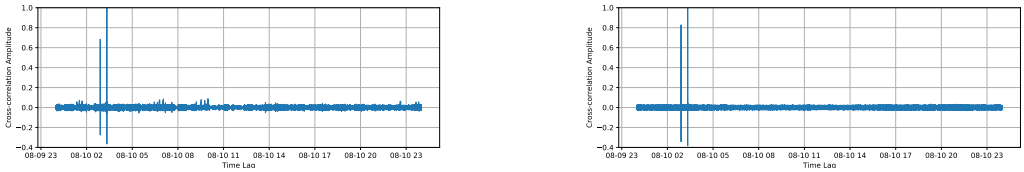

(a) (b)

Figure 5: (a) 2D cross-correlation results between the *Lad#1* data and the continuous recordings on August 10, 2017. The spike with amplitude of 1 corresponds to the *Lad#1*. The other spike with amplitude of 0.7 corresponds to *Lad#2*. *Lad#2* does stand out from the noise. However, there are a few weak spikes that are false positives. (b) results by picking the median of trace-wise cross-correlations at each time lag. The SNR increases evidently. The false positive spikes shown in the 2D cross-correlation results are not apparent. [**ER**]

two panels. Both broadband stations have a higher amplitude of *Lad#2* than SFSO does. However, their noise levels are also higher compared with the SFSO results. For JRSC, the average noise amplitude is approximately 0.121, while the amplitude corresponding to *Lad#2* is approximately 0.9588. SNR for JRSC is approximately 7.90. For JSFB, the average noise amplitude is approximately 0.090, while the amplitude corresponding to *Lad#2* is approximately 0.944. SNR for JSFB is approximately 10.53. For our SFSO array, the average noise amplitude is approximately 0.018, while the signal amplitude is approximately 0.827. SNR for SFSO is approximately 45.97. We can see that with the hundreds of channels to take the median of the results, SFSO array produces higher SNR while at the same time with a less false positive rate compared with the broadband stations.

Figure 7 compares the cross-correlation results on November 27, 2017, the day when *Lad#3* occurred. JRSC is quieter this time and has SNR approximately 16.96. SNRs for SFSO and JSFB are 16.17 and 5.17, respectively. In this case, JRSC performs the best and our SFSO array also performs well. From Figure 3c, we see that the SFSO recording overall has good signal detected. However, the noise level is stronger in a few channels compared to the SFSO recording of *Fl#1* shown in Figure 3a. The higher ambient noise level could explain why the SNR of SFSO results is lower than that obtained from JRSC.

Figure 8 compares the cross-correlation results on January 23, 2018, the day when *Lad#4* (Figure 3d) occurred. Surprisingly, as Figure 8a shows, no signal is detected by the SFSO array. SNRs for JRSC and JSFB are 5.49 and 4.22, respectively. From visually inspecting Figure 3, we can see that the SFSO and JRSF recordings of *Lad#4* shown in Figure 3d have evidently different waveforms compared to the other four events. Thus, it would be reasonable to think of *Lad#4* as a event that originated in the Ladera area but with different mechanisms from the other four events. And from Figure 2, we can see the epicenter of *Lad#4* is an outlier of those Ladera earthquake epicenters, which could also imply that the *Lad#4* has different mechanisms. If

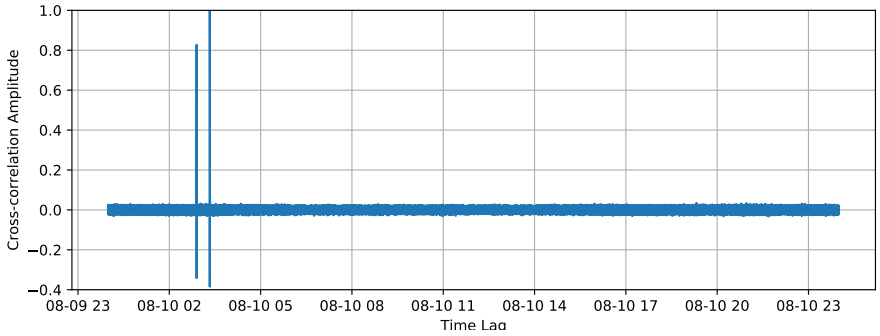

(a)

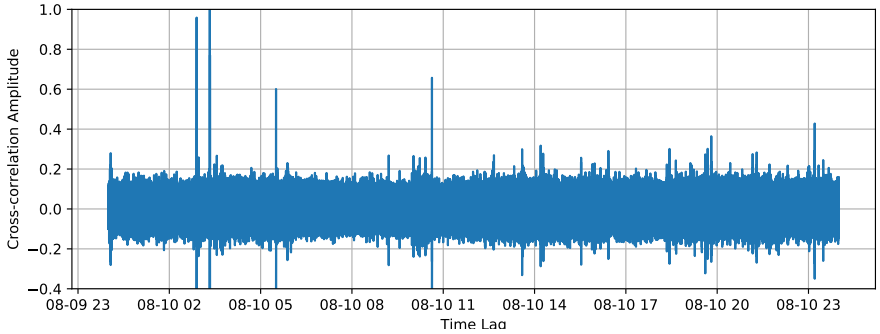

(b)

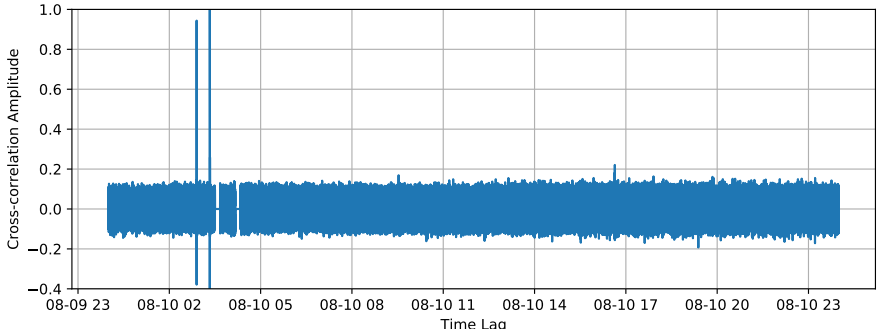

(c)

Figure 6: Cross-correlation results of the recordings on August 10, 2017, the day both *Lad#1* (Figure 3a) and *Lad#2* (Figure 3b) occurred. (a) shows the cross-correlation results of SFSO data; (b) shows the results of the JRSC data. We can see a few false positives; (c) shows the results of JSFB data. In each panel, the spike with amplitude of one corresponds to *Lad#1*, which is the template. The other major spike corresponds to *Lad#2*. The SNRs for SFSO, JRSC and JSFB are 45.97, 7.90 and 10.53 respectively. [**ER**]

this is the case, we can say that our SFSO array is most sensitive to the mechanisms of earthquakes, while JRSC is the least sensitive one.

Figure 9 compares the cross-correlation results on January 11, 2017, the day when *Lad#5* occurred. SNRs for the SFSO array, JRSC and JSFB are 14.37, 15.40 and 4.66, respectively. JSFB has several false positive spikes showing up.

CROSS-CORRELATION WITH THE FELT LAKE TEMPLATE

Figure 10 and Figure 11 show the cross-correlation results of the continuous recordings on July 12, 2017, and July 13, 2017. The two strongest spikes in each panel of Figure 10 correspond to the *Fl#1* and *Fl#2*, respectively. For *Fl#2*, the SNRs of the SFSO array, JRSC and JSFB are approximately 5.39, 3.64, and 6.30 respectively. Our SFSO array has the highest SNR among the three. JSFB has a clear false positive spike approximately at 18:42:00 UTC Time.

In Figure 11, there are two evident spikes in each panel. The two spikes appear in coherent timings across the three instruments. They are all true positives. The spike on the left corresponds to the *Fl#3*. The SNRs for *Fl#3* of SFSO, JRSC and JSFB are 5.06, 3.64 and 3.68 respectively. SFSO has the highest SNR value. The right spike is an event that is not recorded in the USGS catalog. We call it an aftershock (*Fl#5*) of the Felt Lake earthquakes. The SNRs of SFSO, JRSC and JSFB are 3.53, 3.82 and 4.86 respectively. Figure 4e shows the SFSO recording and the vertical components of JRSC and JSFB of *Fl#5*.

In addition to the aftershock event, we found another weak Felt Lake event on May 10, 2017, which is not recorded by the USGS online catalog. Since it occurs before the major Felt Lake earthquake, *Fl#1*, we call it a precursor (*Fl#4*) of the Felt Lake earthquake. Figure 12 shows the cross-correlation results of the SFSO data and the vertical components of the two broadband stations. The spike shown in the SFSO results corresponds to the precursor. In this case, SNRs for SFSO, JRSC and JSFB are 5.56, 4.14 and 4.00 respectively. As can be seen, the SFSO results have the best SNR and no clear false positives.

AMPLITUDE RATIOS OF THE FELT LAKE EARTHQUAKES

Whether or not and how well our SFSO array can estimate magnitudes of the nearby weak events are also our first-order concerns. Herein, we compute the amplitude ratios of the Felt Lake template to the other four Felt Lake events, *Fl#2* through *Fl#5*, for SFSO recordings and the two broadband stations. If the ratios between the different instruments agree with each other, it means that our SFSO array can provide us with a reasonable magnitude estimation. For SFSO, we chose the part

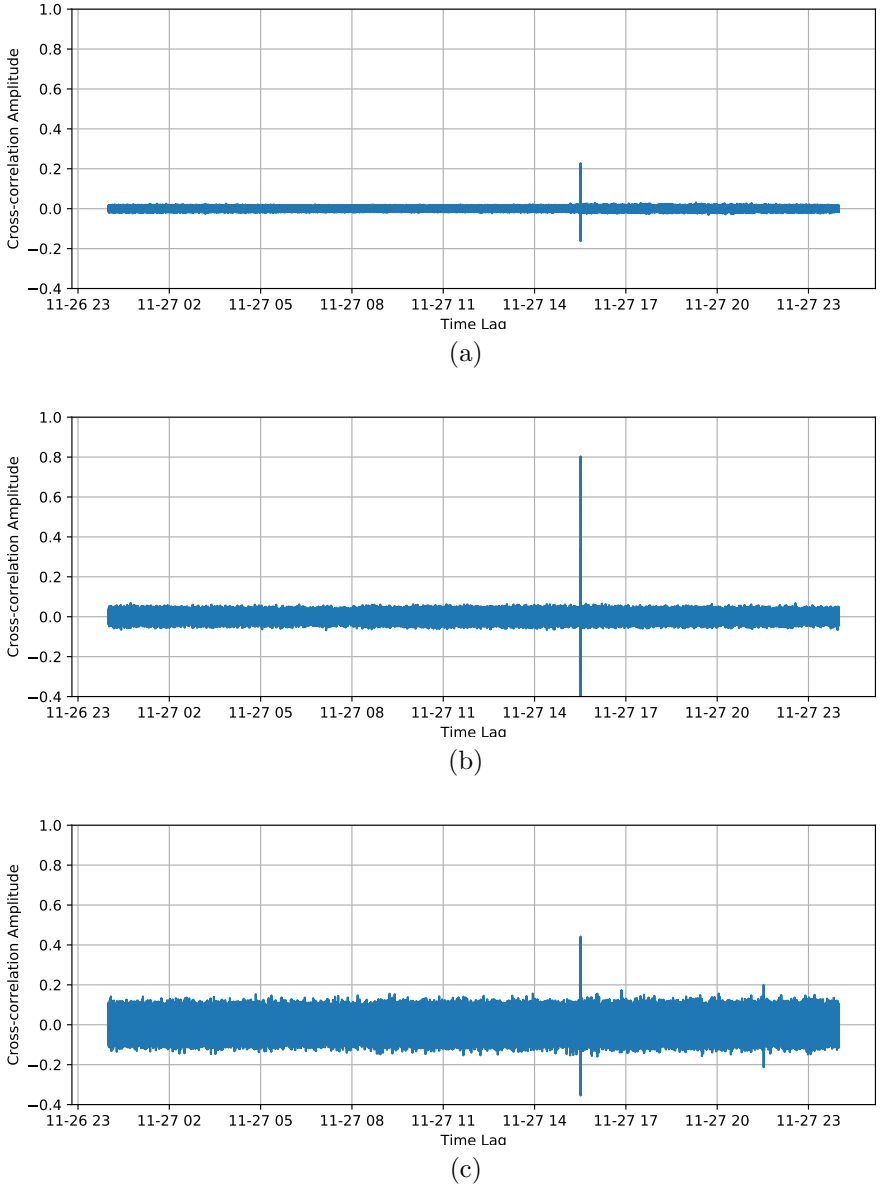

Figure 7: Cross-correlation results on November 27, 2017, the day when *Lad#3* (Figure 3c) occurred. (a) shows the cross-correlation results of SFSO data; (b) shows the results of the JRSC data; (c) shows the results of JSFB data. The SNRs for SFSO, JRSC and JSFB are 16.17, 16.96 and 5.17 respectively. [**ER**]

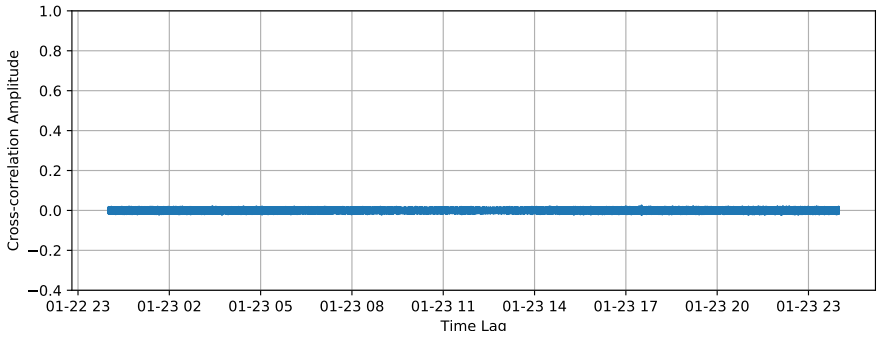

(a)

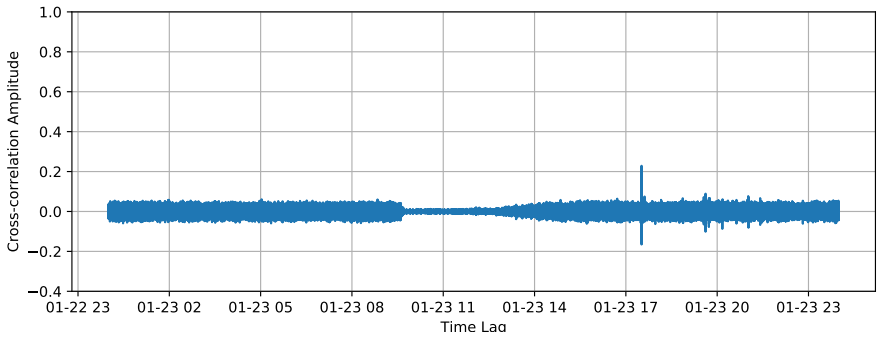

(b)

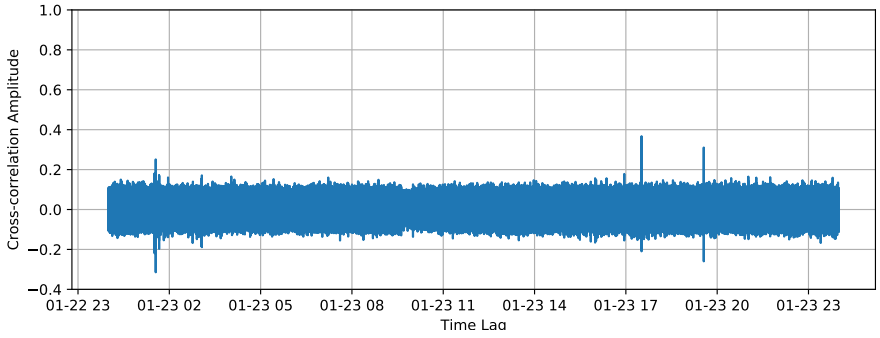

(c)

Figure 8: Cross-correlation results on January 23, 2018, the day when *Lad#4* (Figure 3d) occurred. (a) shows the cross-correlation results of SFSO data; (b) shows the results of the JRSC data; (c) shows the results of JSFB data. SFSO results have no clear signal detected. The SNRs for JRSC and JSFB are 5.49 and 4.22 respectively. [**ER**]

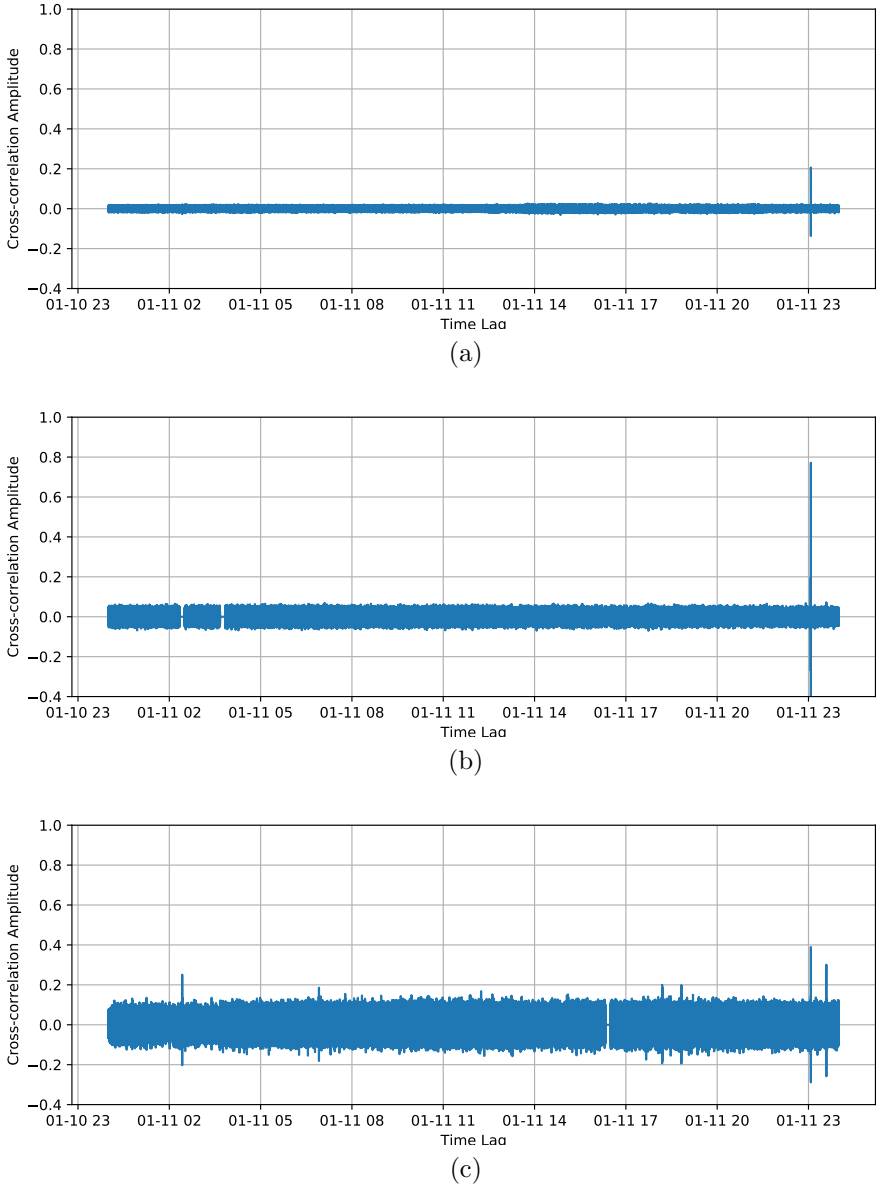

Figure 9: Cross-correlation results on January 11, 2017, the day when *Lad#5* (Figure 3e) occurred. (a) shows the cross-correlation results of SFSO data; (b) shows the results of the JRSC data; (c) shows the results of JSFB data. The SNRs for SFSO, JRSC and JSFB are 14.37, 15.40 and 4.66 respectively. [**ER**]

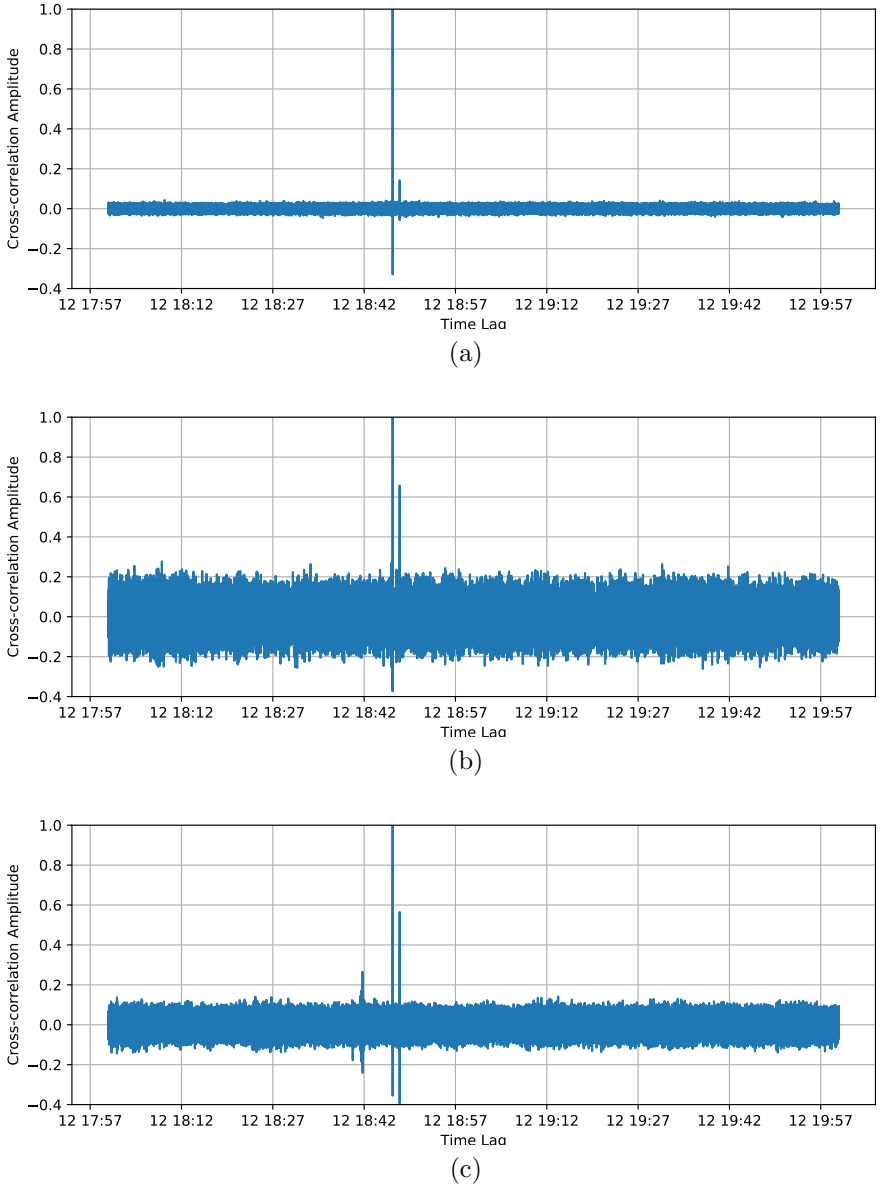

Figure 10: Cross-correlation results on July 12, 2017, the day when *Fl#1* (Figure 4a) and *Fl#2* (Figure 4b) occurred. (a) shows the cross-correlation results of SFSO data; (b) shows the results of the JRSC data; (c) shows the results of JSFB data. For *Fl#2*, SNRs for SFSO, JRSC and JSFB are 5.39, 3.64 and 6.30 respectively. [**ER**]

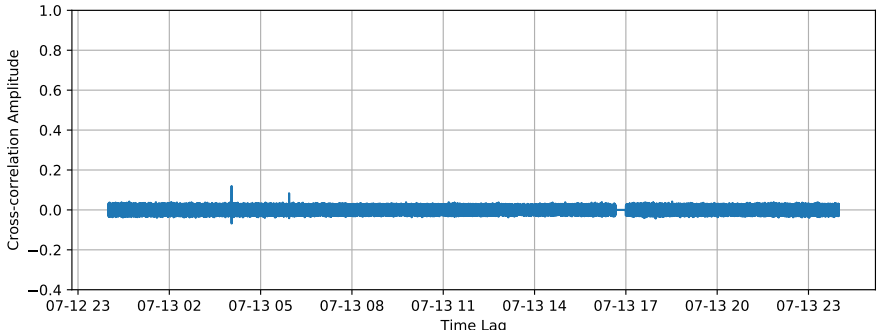

(a)

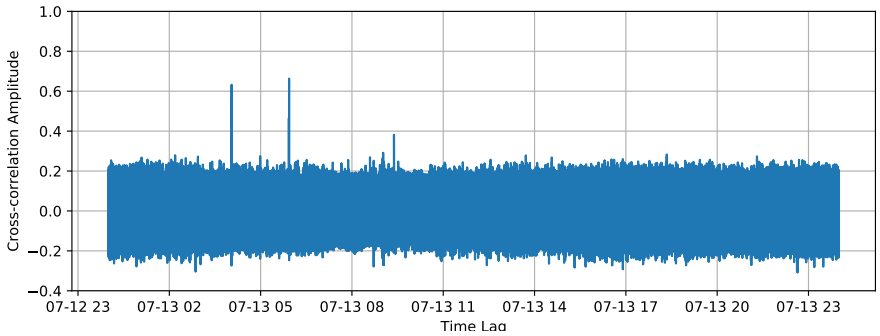

(b)

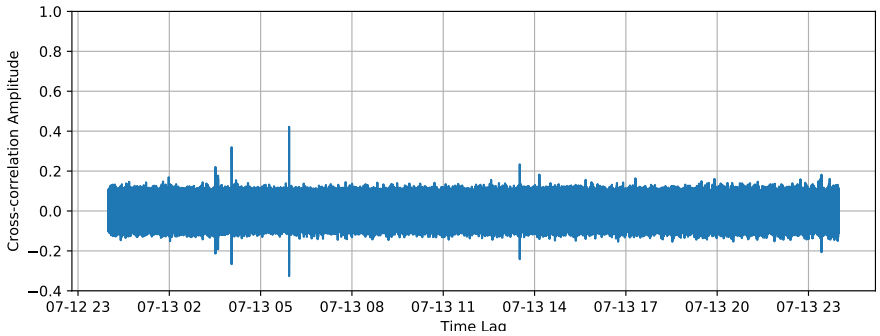

(c)

Figure 11: Cross-correlation results on July 13, 2017, the day when *Fl#3* (Figure 4c) occurred. (a) shows the cross-correlation results of SFSO data; (b) shows the results of the JRSC data; (c) shows the results of JSFB data. There are two spikes shown in (a), the left one corresponds to *Fl#3*. The other one corresponds to the detected aftershock, *Fl#5*(Figure 4e). For *Fl#3*, SNRs for SFSO, JRSC and JSFB are 5.06, 3.64 and 3.68 respectively. For *Fl#5*, SNRs for SFSO, JRSC and JSFB are 3.53, 3.82 and 4.86 respectively. [**ER**]

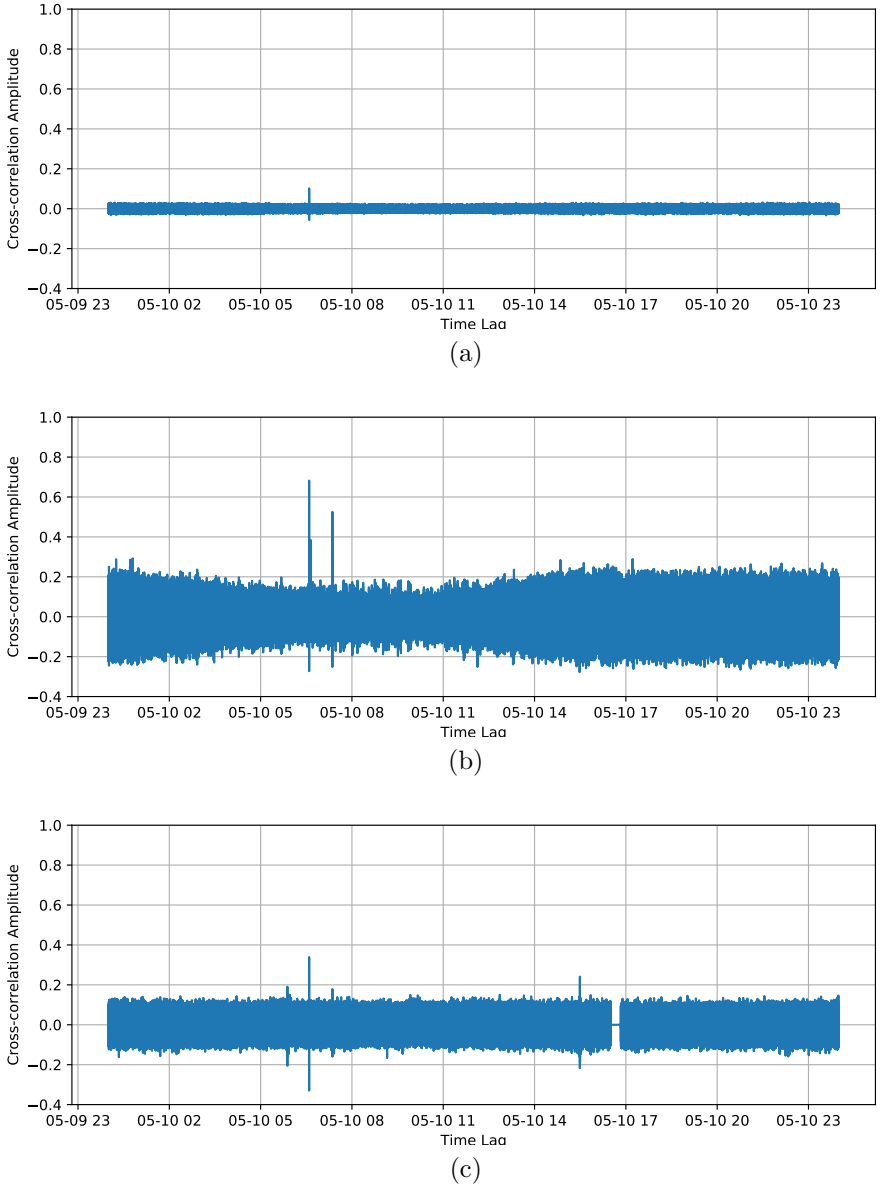

Figure 12: Cross-correlation results on May 10, 2017, the day when the detected precursor, *Fl#4* (Figure 4d), occurred. (a) shows the cross-correlation results of SFSO data; (b) shows the results of the JRSC data; (c) shows the results of JSFB data. SNRs for SFSO, JRSC and JSFB are 5.56, 4.14, 4.00 respectively. [**ER**]

with the orange rectangles (shown in Figure 4) since it contains clear waveforms. For data within the orange rectangles, we set a 80% threshold. We set an absolute value threshold on the weaker events because we do not want to divide the template data by a value close to zero. We set the threshold on the template events because division between relatively great values tends to give us a more reliable ratio estimation. Thus only data points with absolute value greater than the threshold are used to compute the point-wise amplitude ratios. The median of the point-wise ratios are used as the amplitude ratio computed by SFSO data. For broadband stations, we first subtract the median value from the 1D time series; then following similar process as SFSO, for data within orange rectangles, we set a 80% threshold for each of the five events, only data points with absolute value greater than the threshold are used to compute the point-wise amplitude ratios. The median of the point-wise ratios are used as the amplitude ratio computed by broadband data. Because the SFSO recordings used to calculate amplitude ratios correspond to mostly S-wave and surface wave, for a fair comparison, we do not include the P-wave arrivals of the JRSC recordings in the rectangles. However, for JSFB, the P-wave and S-wave arrivals are hard to be differentiated because the epicenters of the Felt Lake events are fairly close to JSFB. Thus, we include the first arrivals of the JSFB recordings in the rectangles. For JRSC data, we did highpass preprocessing by 1.5 Hz to detrend the data.

The following table summarizes the results we obtained. Each column of the table refers to the amplitude ratios of template event (*Fl#1*) to the other four events respectively.

	Fl#2	*Fl#3*	*Fl#4*	*Fl#5*
SFSO	1.66	2.02	2.87	3.98
JRSC	1.92	2.03	3.97	4.72
JSFB	1.67	2.14	3.85	6.09

As the table above shows, all three instruments lead to a same conclusion that, in terms of amplitude, the order of the five events are: *Fl#1* > *Fl#2* > *Fl#3* > *Fl#4* > *Fl#5*. Note that the magnitude of *Fl#1* is estimated in the USGS database to be 1.3. This implies that our SFSO array could contain the information of relative magnitudes between small events. Additionally, we see that our array has the lowest ratios for all of the four events. For *Fl#2* and *Fl#3*, the ratios among the three stations are fairly close. For the two weaker events, *Fl#3* and *Fl#4*, SFSO has more underestimated ratios. This could be explained that our SFSO array has non-linear responses of events with different magnitudes. For events causing weak ground motion, our SFSO array may have a good coupling with the ground. For events with large magnitudes, our SFSO array may have loose coupling with the ground. Therefore, from *Fl#2* to *Fl#5*, the ratios obtained from SFSO recordings decreases. Further investigation is needed to be confirmed.

CONCLUSION AND FUTURE WORK

In conclusion, we show that cross-correlation can be applied on SFSO data as a template matching method to detect earthquakes. Comparing to the cross-correlation results obtained from the nearby broadband stations, we show that SFSO results have higher or similar SNR level with no evident false positives due to the advantage of the dense channel distribution, which means our SFSO array has a good sensitivity of the nearby weak events. Additionally, with the cross-correlation results for *Lad#4*, we show that the SFSO array is more sensitive to events with different mechanisms. From analyzing the amplitude ratios between the *Fl#1* and the other four detected Felt Lake earthquakes, we show that all three instruments get the same amplitude order. The amplitude ratios agree with each other well for the two relative large events, *Fl#2* and *Fl#3*. For *Fl#4* and *Fl#5*, our SFSO array tends to underestimate the ratios, which could be explained that our SFSO array has non-linear responses of events with different magnitudes.

The future work would be to keep exploring a way of increasing the SNR of the SFSO array taking advantage of the dense channel distribution of the SFSO array. One way could be performing cross-correlation or other template matching algorithms on the six segments independently, because each segment could have different data quality due to their different locations. Performing analyses independently could prevent us from being biased by some segments with particularly poor SNR. Then, we would perform cross-correlation with various template recordings (with various magnitudes) to understand the detection capacity of our SFSO array and how well we can estimate event magnitudes from computing amplitude ratios of SFSO data.

ACKNOWLEDGEMENT

We would like to thank OptaSense Ltd for making the SFSO recording equipment available. We thank Martin Karrenbach, Steve Cole and our colleagues at Stanford for helpful discussions and insights.

REFERENCES

Biondi, B., E. Martin, S. Cole, and M. Karrenbach, 2017, Earthquakes analysis using data recorded by the Stanford DAS Array: SEP-Report, **168**, 11–26.

Li, Z. and Z. Zhan, 2018, Pushing the limit of earthquake detection with distributed acoustic sensing and template matching: a case study at the brady geothermal field: Geophysical Journal International, **215**, 1583–1593.

Martin, E., B. Biondi, S. Cole, and M. Karrenbach, 2017a, Overview of the Stanford DAS Array-1 (SDASA-1): SEP-Report, **168**, 1–10.

Martin, E. R., C. M. Castillo, S. Cole, P. Sawasdee, S. Yuan, R. Clapp, M. Karrenbach, and B. L. Biondi, 2017b, Seismic monitoring leveraging existing telecom

infrastructure at the sdasa: Active, passive, and ambient-noise analysis: The Leading Edge, **36**, 1025–1031.

Yuan, S., E. R. Martin, J. P. Chang, S. Cole, and B. Biondi, 2017, Catalog of Northern California earthquakes recorded by DAS : SEP-Report, **170**, 81–96.